Light harvesting dynamics in desert crust cyanobacteria: Changes in aggregation state as a mechanism for modulating energy transfer

Leeat Bar-Eyal[1], Reza Ranjbar Choubeh[2], Eyal Cohen[1], Ido Eisenberg[1], Carmen Tamburu[1], Márta Dorogi[3], Renáta Ünnep[3], Marie-Sousai Appavou[4], Reinat Nevo[5], Uri Raviv[6], Ziv Reich[5], Győző Garab[3], Herbert van Amerongen[7], Yossi Paltiel[6], Nir Keren[1]

[1]The Hebrew Universtiy of Jerusalem, [2]Wageningen UR, [3]Hungarian Academy of Sciences, [4]Forschungszentrum Jülich GmbH, [5]Weizmann Institute of Science, [6]The Hebrew University of Jerusalem, [7]Wageningen University

Submitted to Proceedings of the National Academy of Sciences of the United States of America

In this paper we propose an energy dissipation mechanism that is completely reliant on changes in the aggregation state of the phycobilisome light harvesting antenna components. All photosynthetic organisms regulate the efficiency of excitation energy transfer (EET) to fit light energy supply to biochemical demands. Not many do this to the extent required of desert crust cyanobacteria. Following pre-dawn dew deposition, they harvest light energy with maximum efficiency until desiccating in the early morning hours. In the desiccated state absorbed energy is completely quenched. Time and spectrally resolved fluorescence emission measurements of the desiccated desert crust *Leptolyngbya ohadii* strain identified (a) reduced EET between phycobilisome components (b) shorter fluorescence lifetimes (c) red shift in the emission spectra, compared to the hydrated state. These changes coincide with a loss of the ordered phycobilisome structure, evident from small angle neutron and X-ray scattering and cryo-TEM data. Based on these observations we propose a model where in the hydrated state the organized rod structure of the phycobilisome supports directional EET to reaction centers with minimal losses due to thermal dissipation. In the desiccated state this structure is lost, giving way to more random aggregates. The resulting EET path will exhibit increased coupling to the environment and enhanced quenching.

photosynthetic efficiency | cyanobacteria | desiccation | phycobilisome | energy dissipation

Introduction

Deserts cover almost half of the Earth's terrestrial surface, and although desert conditions may seem unfavorable, they are home for diverse ecosystems. Many of these ecosystems are founded on biological desert crusts, which play an essential role in stabilizing shifting sands and enriching them with nutrients (1, 2). Cyanobacteria are among the first microorganisms to inhabit these crusts where one of the major sources of water is often dew deposited before dawn (3, 4). However, as temperatures elevate water quickly evaporates. Such conditions can be extremely harmful for photosynthetic organisms, and require adaptations on all cellular levels (3–9). These include shifts in metabolic profiles and the accumulation of compatible solutes. A key issue is the adaptation of the photosynthetic apparatus, since continued photosynthetic activity under high light, and especially in combination with desiccation may lead to the production of reactive oxygen species that will cause damage to the entire cell (10–12). The cyanobacteria that colonize sand crusts evolved strategies for coping with these daily cycles of hydration using mechanisms that enable extensive quenching of absorbed light energy. The extent of quenching in these organisms far exceeds that of common laboratory model organisms (13, 14).

Our studies focused on *Leptolyngbya ohadii*, a crust cyanobacterium isolated from the Nizzana region of the NW Negev desert in Israel (3, 6). This is a keystone organism in this environment (4). To maintain *L. ohadii* cells in a viable state the desiccation process must be gradual (3). Recovery of photosynthetic activity, on the other hand, can occur immediately upon the addition of water (7). The desiccation/hydration transition does not require the break down and renewed production of photosynthetic protein complexes or pigments, and allows *L. ohadii* to utilize the short time of morning hydration for photosynthesis and avoid photo-damage during the remainder of the day (4).

A study of this process indicated similar absorption cross sections for desiccated and hydrated cyanobacteria *i.e. L. ohadii* absorbs a similar amount of light energy per wavelength when hydrated and when desiccated (7). Nevertheless, in the desiccated state electron transport is shut down and fluorescence yield decreases by ~70%. This requires efficient dissipation of excess energy to heat during desiccation together with a mechanism for fast energy distribution. We found evidence for a block in electron transport and dissipation of excitation energy through the accumulation of a stably oxidized P_{700} (primary photosystem I photochemical center). Oxidized chlorophylls are strong quenchers. Shrinkage of the lumenal space, observed in TEM, and restriction of plastocyanin diffusion provide a possible mechanism for the accumulation of P_{700}^{+}. However, this is not the only protective mechanism at play in the desiccated state. Our data also indicated

Significance

All photosynthetic organisms regulate efficiency of excitation energy transfer (EET) to fit energy supply to biochemical demands. For desiccation tolerant desert crust cyanobacteria this ability is of the utmost importance. These organisms spend most of the daytime in the desiccated state whence absorbed energy is completely quenched. Based on our observations we propose a model where in the hydrated state the organized rod structure of the light-harvesting phycobilisome supports directional EET to reaction centers with minimal losses to thermal dissipation. In the desiccated state this structure gives way to more random aggregates. The resulting EET path exhibits increased coupling to the environment and enhanced quenching. This energy dissipation mechanism is completely reliant on changes in aggregation state of phycobilisome components.

Reserved for Publication Footnotes

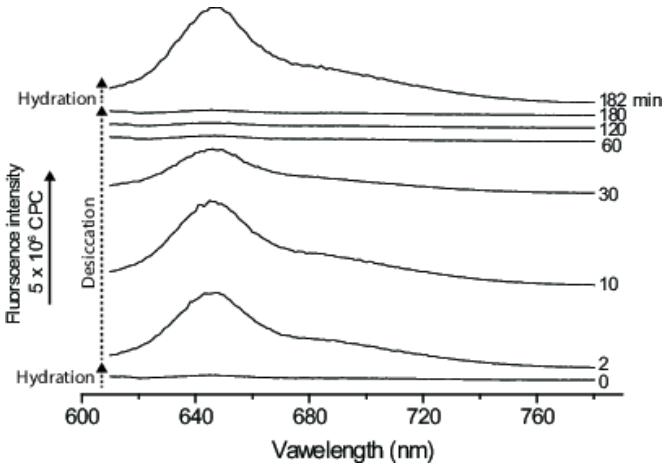

Fig. 1. Reversibility of fluorescence yield during desiccation and rehydration. A desiccated*L. ohadii* culture was exposed to two cycles of desiccation and rehydration. Fluorescence spectra were measured with an excitation wavelength of 580±2 nm. The traces are baseline shifted. The fluorescence trace of the desiccated sample did not exhibit any discernible peaks (0 min curve). However, immediately after rehydration PBS fluorescence was observed (2 min). The peak is dominated by PC fluorescence at 650 nm and contains a 670 nm APC shoulder. The filter was then desiccated for 180 min (2 min to 180 min), before a second rehydration round. Again, an immediate recovery of PBS fluorescence was observed (182 min).

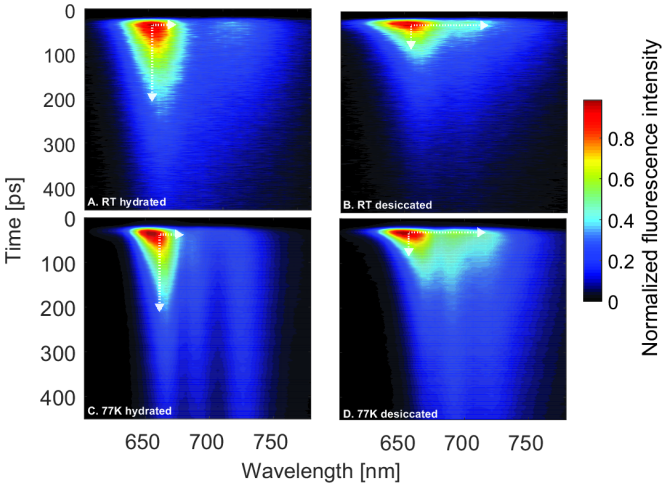

Fig. 2. Propagation of photosynthetic fluorescence following 580 nm excitation with picosecond time resolution and spectral information. Panels A and B present data for room temperature measurements. Panels C and D present 77K measurements. The fluorescence intensity was normalized (from 0 to 1), the scale is presented on the right hand side.In the desiccated samples we observe a shortening of the lifetime and a redshift of the fluorescence, as compared to the hydrated sample. The differences are highlighted by white dashed arrows. In the hydrated state at 77K, three spectral features emerge: ~650-670 nm, ~670-700 nm, ~720-750 nm. These are normally ascribed to PBS, PSII and PSI fluorescence, respectively. However, we observed fluorescence at wavelengths >700 nm in isolated *L. ohadii* PC (Fig. S2).

a strong quenching reaction in the phycobilisome (PBS) light-harvesting antenna (7).

PBSs are assembled by the association of phycobiliproteins (PBPs) to which linear tetrapyrroles are covalently linked. Typically, PBS cores contain cylinders made up of hexamers of the lowest energy absorbing PBP variant, allophycocyanin (APC; λ_{max}= 650 nm). PBS rods can be composed of a number of different PBPs (15). In the case of *L. ohadii* the rods contain phycocyanin (PC; λ_{max}= 620nm).

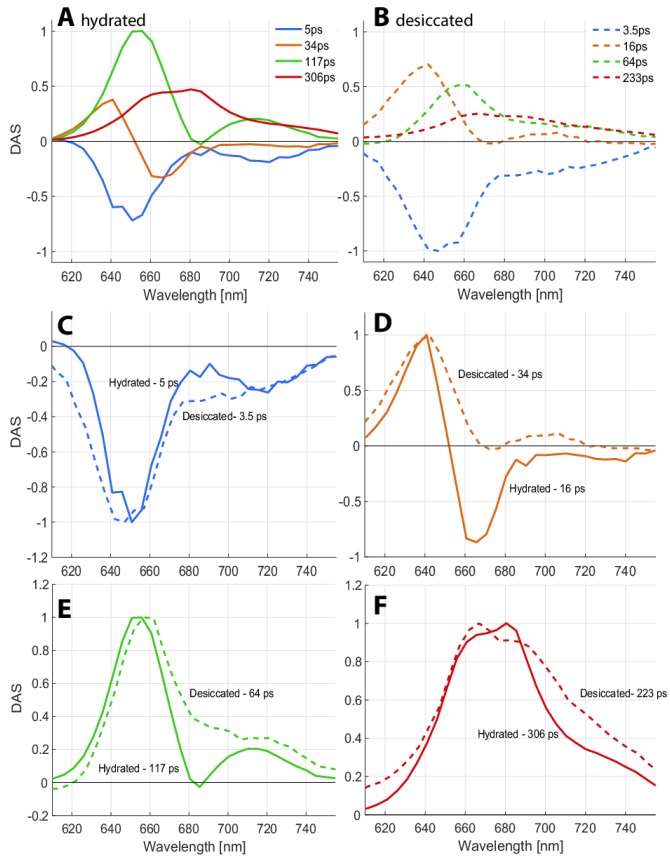

Fig. 3. Global analysis of desiccated and hydrated states spectrally-resolved picosecond fluorescence. DAS and corresponding fluorescence lifetimes of hydrated (A) and desiccated (B) samples. Panels C-F present a comparison between the corresponding normalized DAS of hydrated and desiccated components. Each DAS is marked by its corresponding lifetime. The DAS of desiccated cells are dashed. A summary table for the observed lifetime ranges in 3-4 repeats is included in Table S1. In addition to DAS, the data was analyzed using a sequential model and the obtained EAS is presented in Fig. S1.

In this study we dissected PBS fluorescence quenching processes in *L. ohadii.* We performed spectroscopic measurements on both hydrated and desiccated samples of *L. ohadii*, in order to uncover energy transfer pathways between components of the PBS system in the different states. Structural organization of the inter-thylakoidal space was examined by neutron and X-ray diffraction techniques. The results suggest a different excitation energy transfer (EET) path within the PBS antenna in hydrated and desiccated samples. The desiccated samples' EET path exhibits an efficient widespread quenching effect, resulting from interactions of PBS pigments.

Results

Under laboratory conditions *L. ohadii* is able to retain viability for prolonged periods and regain photosynthetic activity immediately after rehydration. We have demonstrated this in the past for electron transfer activity (7). Fig. 1 demonstrates this remarkable ability for PBS function. A desiccated culture, in which PBS fluorescence was strongly quenched, regained its high fluorescence yield as soon as 2 min after rehydration. The hydration/desiccation process was completely reversible. After ~2 h, at ambient temperature, the culture was desiccated and fluorescence was quenched. Rehydration resulted in immediate recovery (Fig. 1).

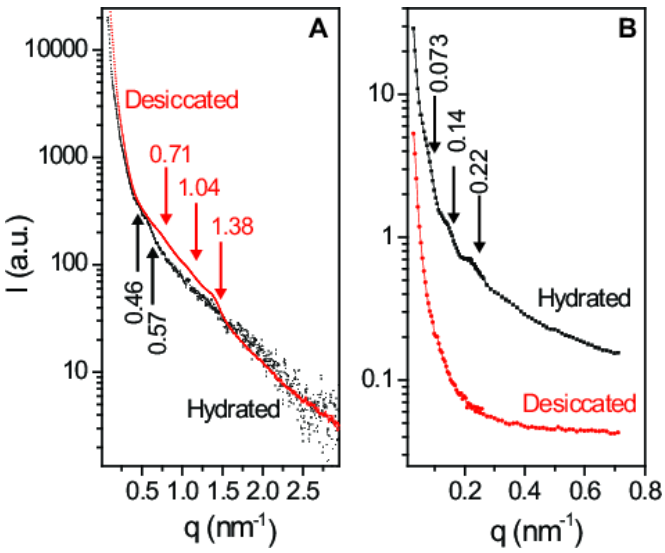

Fig. 4. Small-angle X-ray and neutron scattering measurements. Hydrated and desiccated samples were studied by solution small-angle X-ray scattering (SAXS, A) and small-angle neutron scattering (SANS, B). The data presented were azimuthally integrated from the 2D raw data and plotted as intensity as a function of the magnitude of the scattering vector, q. In both cases, several weak intensity peaks were observed (indicated by arrows). On the right panel, azimuthally integrated SANS scattering curves were measured at 20 m (hydrated sample) and overlapped 20 m and 8 m (desiccated sample) sample-detector distances. The line represents the fitted curve (linear combination of a constant, and a power function and three Gaussians). No peak could be detected between 0.35 and 3.5 nm^{-1} on SANS curves. The first-order q value of the features observed in the measurements can be translated into a repeat distance RD=2π/q. Prominent features are marked directly on the graphs.

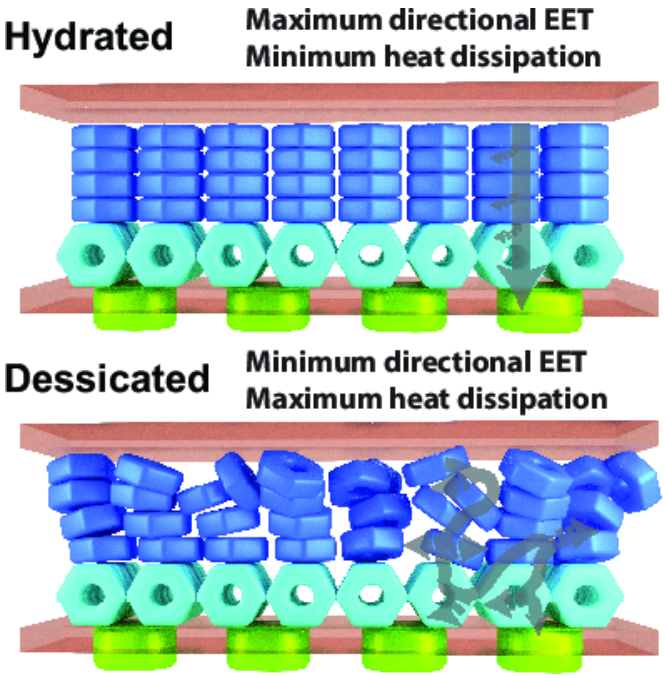

Fig. 5. Model for EET processes in the hydrated and desiccated states. A schematic representation of the aggregation state of the PBS antenna in both states. The components are drawn roughly to scale. Green – photosystems, cyan – APC, blue – PC, gray arrows – directional EET, dashed arrows – heat dissipation. In the crowded inter-thylakoidal space only small changes in aggregation state are possible, these were exaggerated in the figure for demonstration purposes.

To understand the energy transfer dynamics controlling this process we conducted measurements using a streak-camera system that provides picosecond time resolution as well as spectral information. Measurements were performed on *L. ohadii* samples in the desiccated and the hydrated states. The excitation wavelength was set to 580 nm, exciting mainly the PC component of the PBSs (15, 16). Fig. 2 presents an example of the raw data collected at room temperature (A & B) and at 77 K (C & D) from hydrated and desiccated samples. Measurements conducted at room temperature best represent natural conditions. Measurements at 77 K allow better spectral resolution of the various fluorescence peaks.

Several differences appear very clearly when comparing the raw room temperature data of the two states (highlighted by the arrows in Fig. 2). The first is the shortening of the desiccated sample's florescence lifetime across all wavelengths. The second prominent difference is the wavelength broadening of the desiccated sample fluorescence spectrum towards the red, as compared to the hydrated sample. These observations are in line with the lower resolution Time-Correlated-Single-Photon-Counting (TCSPC) data in (7). The temporal and spectral resolution of the measurements reported here provide an opportunity to examine faster processes, occurring before thermal equilibration.

To resolve both spectral and temporal components, global analysis (17) was conducted on the data (Fig. 3; analysis by Evolution Associated Spectra (EAS) (17) is presented in Fig. S1). Table S1 summarizes the lifetimes of the various components. The best minimal fit for the data was obtained with four fluorescence decay lifetimes.

The 5 ps and 3.5 ps decay-associated spectra (DAS) of hydrated and desiccated samples respectively (Fig. 3A and 3B) reflect excitation equilibration following absorption at 580 nm. The 5 ps DAS obtained for the hydrated sample is negative at all wavelengths. One of the peaks of this 5 ps DAS is located at 650 nm and the other is located around 700-720 nm (Fig. 3C). The lifetime (τ) and the DAS shape are rather similar to those observed in the laboratory model organism *Synechocystis* sp. PCC 6803 (16). In the desiccated sample the resolved lifetime of the above component is somewhat shorter (Table S1). The difference in the lifetimes of the 3.5 and 5 ps DAS is insignificant because the full width at half maximum (FWHM) of the instrument response function (IRF) is around 3.5-5 ps and this limits resolving a clear difference between these two short lifetimes. The shape of the 3.5 ps and 5 ps DAS of the desiccated and hydrated states show significant differences. In the desiccated state the ~650 nm peak is broader and, instead of a distinct peak at ~720 nm, a broad shoulder extending from 680 nm to 740 nm is observed (Fig. 3).

In steady-state measurements, isolated PC from *L. ohadii* exhibited two peaks: one centered at ~650 nm and another broader peak at ~685 nm. The latter extends well beyond 700 nm (Fig. S2). Similar steady-state spectra were observed in PC from other cyanobacterial species (see for example (18, 19) and many others). Based on the similarities with the *in vitro* data we attribute the first DAS component to PC EET. However, these are *in vivo* measurements and the possibility of emission from photosystem I (PSI) cannot be excluded. A significant contribution of PSI is, however, unlikely considering the 580 nm excitation wavelength.

The 34 ps DAS in the hydrated state shows a positive peak at ~640 nm and a negative peak at ~660 nm, indicating energy transfer from ~640 nm to ~660 nm (Fig. 3D). This DAS was previously attributed, in a laboratory model cyanobacterium, to internal PBS energy transfer *i.e.* from PC to PC and from PC to APC_{660} (16, 20). The corresponding DAS in the desiccated state has a lifetime of 16 ps (Fig. 3D), which is markedly different from the 34 ps DAS in the hydrated state. While the 34 ps DAS of the hydrated state shows EET, the 16 ps DAS of the desiccated state lacks a clear negative amplitude, indicating a major reduction of the corresponding EET process.

The 117 ps DAS in the hydrated state partly reflects EET from APC_{660} to the terminal emitter APC_{680} or to chlorophylls fluorescing at 680 nm (16). The 64 ps DAS of the desiccated state lacks a negative peak indicating the absence of EET compared to the hydrated state. The EAS of this component show a prominent red shift and broadening of the desiccated state spectrum (Fig. S1).

The 306 ps DAS of the hydrated state and the 233 ps DAS of the desiccated state represent the disappearance of an equilibrated excitation distribution over all of the components of the system, namely PC, APC_{660}, APC_{680}, and chlorophylls. It is faster for the desiccated state and both DAS and EAS indicate a stronger contribution on the long-wavelength side.

The comparison between the desiccated and the hydrated fluorescence kinetics indicates (a) significantly reduced downhill EET (Fig. 3D and 3E) towards the RCs and (b) a substantial decrease of the fluorescence lifetimes, meaning that an additional non-radiative decay pathway has been created.

To test this further we performed measurements at 77 K (Fig. 2). A detailed description of the DAS decomposition is included in Fig. S3. At 77 K the fluorescence lifetimes of both hydrated and desiccated states are longer compared to room temperature. Furthermore, the differences between the desiccated and hydrated samples are smaller. Global analysis results indicate the convergence of both DAS shapes and lifetimes (Fig. S3). At 77 K PSI and photosystem II (PSII) fluorescence can be resolved. Nevertheless, in the desiccated samples the DAS decomposition indicates reduced EET from the PBSs to both photosystems.

The analysis of the measurements performed at room temperature and 77 K support the existence of a fast heat dissipation pathway in the desiccated state. This channel is apparently far more efficient at room temperature than at 77 K. Quenching of excitation energy might be explained by the function of the orange carotenoid protein (OCP). OCP is photoactivated by high blue-green irradiance, binds to APC and leads to the dissipation of excess energy absorbed in the PBSs under high-light conditions (21, 22). However, OCP is not a likely candidate for the non-radiative dissipation observed in the desiccated state. The extent of fluorescence quenching measured in desiccated *L. ohadii* is much larger (Fig. 1) than that induced by OCP in other cyanobacteria (e.g. (16, 22–24)). Moreover, OCP binds and facilitates energy dissipation by interaction with the APC core (25). However, in the desiccated state we observed only little, if any, energy transfer from PC to APC. Furthermore, the overall effect of OCP knockout or over-expression on results of streak camera measurements is much smaller and focused to APC (16).

We can consider two additional alternatives for the mechanism underlying the activity of the dissipation pathway. The first is a change within the structure of PBS pigment-protein complexes. Such a change can, for example, enhance charge transfer reactions between a bilin pigment and an adjacent amino acid, as demonstrated in the FMO (green sulfur bacteria antenna protein) and isiA (cyanobacterial iron stress induced antenna protein) chlorophyll binding proteins (26, 27). The second is a change in the aggregation state of the PBS proteins leading to the generation of intermediate-coupling interactions between them.

The visible absorption spectra of hydrated and desiccated samples did not show any significant difference in cross section or in line shape (7). Additional CD measurements, in the visible range, failed to detect significant differences as well (Fig. S4). These data do not provide evidence for a major change in the energetic properties of the individual pigments in the hydrated and desiccated states. Furthermore, EPR spectroscopy did not detect a radical that can be associated with a charge transfer reaction in the desiccated state (7).

On the other hand, previous cryo-TEM studies of the ultrastructure of the inter-thylakoidal space harboring the PBSs did indicate differences between the two states (7). In the hydrated state the inter-thylakoidal space was well organized with uniform repeat distances and apparent rod structures traversing it. Such PBS architecture was also observed in *Acaryochloris marina* as well (28). Interestingly, both species effectively grow as biofilms. The well-organized architecture is lost in the desiccated state (an example of the TEM observations is included in Fig. S5). Additional ultrastructural information was gained through small angle X-ray and neutron scattering experiments (SAXS and SANS, Fig. 4). These techniques were used in a number of studies to measure the repeat distances (RDs) in different thylakoid membrane systems *in vivo* and *in vitro* (29–31). While providing 1D information, they do not require freezing or fixation.

Both SANS and SAXS scattering profiles carry information about key structural parameters, such as RDs of periodically organized multilamellar membrane systems, but with different sensitivities. The SAXS signal arises from differences in the electron density distribution while SANS is sensitive to protons. In the presence of D_2O, SANS allows distinguishing scattering length density between the aqueous regions and the lipid membrane (32). Also, SANS can usually measure in smaller q ranges than SAXS. Accordingly, SAXS data provides information on relatively smaller intra-thylakoidal RDs between electron densities defined by proteins and the lipid bilayer *e.g.* in the lumenal space, whereas SANS data provides information on the RD of thylakoid membranes.

In the hydrated sample SAXS features are observed at q=0.46, 0.57 nm^{-1} (Fig. 3A). These features are replaced by ones with higher q values in the desiccated state (0.71 and 1.04 nm^{-1}; q=1.38 nm^{-1} might be the second harmonics of the principal peak at q=0.71 nm^{-1}). These q values can be interpreted as decreased width of the thylakoid envelope in the desiccated state, which shrinks from 11-14 nm to 6-9 nm.

SANS data reported a feature at q=0.072 nm^{-1} with two additional higher harmonic features at 0.139 and 0.221 nm^{-1}. These values can be interpreted as the RD≈87 nm of the inter-thylakoidal space. This is slightly larger than reported for *Synechocystis* 6803 (80 nm in (32) and 60 nm in (31)) and might indicate larger light harvesting antennae. In the desiccated state these characteristic features are almost completely lost. The scattering intensity decreased dramatically due to the loss of water. No Bragg peak could be discerned between 0.05 and 0.1 nm^{-1}; instead, a broad shoulder emerged between 0.10 and 0.15 nm^{-1}, which can be assigned to a broader range of inter-thylakoidal RDs.

The SAXS and SANS data fit well with cryo-TEM of hydrated and desiccated *L. ohadii* (Fig. S5, the complete analysis is in (7)). In the desiccated state, TEM images indicated a ~50% decrease in lumenal space, a value that is in line with the reduced RD observed in SAXS. This shrinkage was suggested to contribute to the PSI-based quenching mechanism (7, 33). They also indicated a loss of the organized thylakoid membrane space and of the apparent rod structures in the inter-thylakoidal space, which is in line with the SANS observations. Taken together cryo-TEM, SANS and SAXS support a change in the organization of the inter-thylakoidal space and in the aggregation state of the PBSs that populate it.

Discussion

In the desiccated state we observed (a) reduced EET between PBS components (b) extensive heat dissipation (c) fluorescence red shift (Fig. 2-3, Fig. S1-3). These changes coincide with a loss of the organized PBS structure in the inter-thylakoidal space (Fig. 4, Fig. S4-5).

How could a change in the aggregation state of PBSs support a transition between highly efficient EET and quenching? We can

draw corollaries from *in vitro* studies in which we controlled the aggregation state of PC and APC artificially (34). Aggregation of PC in solution leads to shortening of their lifetime, red shift and a lower fluorescence yield. This was a reversible process that occurred in the absence of any additional auxiliary quenching proteins, such as OCP. The effect of aggregation on APC was much smaller.

It is important to note that aggregates discussed here are not chromophore aggregates but rather aggregates of chromophore-containing proteins. Unlike artificial cyanine and porphyrin aggregates, phycobilisomes represent a different scenario. Pigment distances within PC and APC subunits and between them dictate intermediate coupling strength (35, 36).

The underlying mechanism proposed is based on the intermediate-length (1-2 nm) coupling interactions between PC units through the external β155 pigments. A random network of intermediate coupling through the PC aggregates will generate long and convoluted EET paths and a band gap structure with many localized states that couple well to the wide frequency of environmental thermal "noise" (37, 38). In an intermediate coupling regime the band structure strongly depends on the level of disorder of the system, the splitting between bands is smaller and the gap is less protected. Such a structure will support decay to the lowest energy pigments together with quenching through an increased probability for interactions with the thermal bath. In APC, which lacks the external β155 pigments, the chances for generating a network of intermediately coupled trimers are smaller and so are the effects of its aggregation state on EET.

PC is known to be sensitive to the ionic or dielectric properties of its environment (34). However, changes in these properties during desiccation are not expected to lead to the dramatic fluorescence quenching observed here (Fig. 1). Our data indicates small changes in the aggregation state with no detectable difference in the optical properties of the PC units themselves. We propose an *in vivo* model where in the hydrated state the organized rod structure supports directional EET to the RCs with minimal losses due to thermal dissipation (Fig. 5). In the desiccated state, this structure is lost, giving way to less organized aggregates. These less organized *in vivo* aggregates will exhibit EET properties similar to those of *in vitro* PC aggregates – with better coupling to wide frequency environmental noise (37). This type of mechanism can also explain the temperature effect. In tightly coupled pigment networks (in Light Harvesting Complex II or FMO, for example, (39–42)) the energetic differences between 300 K and 77 K are too small to affect EET. Under an intermediate coupling regime, however, these temperature differences are expected to have a larger effect (43, 44). A mechanism based on small and localized changes in aggregation of PBS components in the crowded inter-thylakoidal space may explain the very fast rate of response to rehydration (Fig. 1).

The mechanism suggested here is akin to that proposed by Tamary and coworkers for high light induced quenching in *Synechocystis* 6803 where local heat transients generated in the PBSs by non-radiative energy dissipation were suggested to be the source of the non-photochemical quenching (NPQ) phenomenon (45). Furthermore, the idea that changes in the aggregation state can control the efficiency of EET in the photosynthetic antenna was considered as a mechanism for NPQ in plants. *In vitro* studies demonstrated that aggregation of Light Harvesting Complex II (LHCII) antenna complexes leads to efficient energy dissipation (46–51), although the significance of changes in LHCII aggregation state for energy dissipation *in vivo* is still debated (52, 53). It is important to note a number of key differences between LHCII and PC. (a) LHCII is trapped in the membrane. Its range of possible aggregation geometries is limited to the membrane plane. (b) The pigment-pigment distances within LHCII are, on average, shorter than within PC – supporting a tighter excitonic coupling regime. (c) LHCII contains carotenoids, dedicated to quenching. These are missing from PC. An aggregation based mechanism creating a network of intermediately coupled pigments and, henceforth, increased coupling to the thermal noise is much more likely in cyanobacteria than in vascular plant antennae.

Desiccation and rehydration in photosynthetic organisms are complex processes that require protection of many cellular processes, first and foremost, of the photosynthetic apparatus. The rate of recovery from desiccation is highly variable ranging from days in the case of certain vascular plants (54) to a few seconds in the case of desert crust cyanobacteria. So far, we were able to uncover two mechanisms for blocking photosynthetic activity in the desiccated state: constriction of the lumenal space leading to a block of plastocyanin diffusion, and accumulation of P_{700}^{+} (7) and changes in the aggregation state of PBS components, as discussed here. In both cases the quenching mechanism relies on the rearrangement of existing components of the photosynthetic apparatus. In the new mechanism proposed here we also suggest a method for distributing the energy through a PC aggregate. It is the combination of all features of this desiccation mechanism that allows the very rapid response to rehydration.

Evidence for EET processes at the quantum/classical border are emerging from several studies of the photosynthetic apparatus and are highly relevant for new technologies. Here, small changes in configuration of an intermediately coupled pigment network supports a switch from highly efficient energy transfer to quenching (Fig. 5). In most cases, nano-scale technologies focus on energy transfer devices with tight coupling and low environmental noise (low temperatures) (55). The design principles of the desiccating PBSs suggest a new approach that will enable room temperature devices that can be switched to efficient energy transfer. By utilizing these principles it will be possible to develop a coupling controlled nano-toolbox for various future technologies including computers, materials and sensors.

Materials and Methods

Culture growth and preparation for measurement

Leptolyngbya ohadii cultures were grown (as described in (7)) in YBG11 medium in shaking flasks at 30 °C and 60 μmol photons m^{-2} s^{-1} provided by fluorescent lamps. Cells were homogenized and filtered on 0.45 μm nitrocellulose (NC) filters. For measurement of dry samples, "artificial crust" filters were left to air dry at room temperature for at least two hours.

Steady-state fluorescence measurements

Samples were desiccated on the surface of a NC filter. The filter was mounted on a glass slide and fitted into the measurement chamber of a Fluoromax3 spectrofluorometer (Jobin Yvon). Hydration was performed *in situ*.

Time-resolved fluorescence measurements

Room temperature time-resolved fluorescence spectra were measured using a picosecond streak-camera set-up (56) as described in (16). The excitation wavelength was set to 580 nm, in order to preferentially excite the PBSs. 77 K measurements were performed as described in (57). Measurements were made on either desiccated or hydrated filters of *Leptolyngbya ohadii*, and each measurement was repeated 2-4 times, measuring a different spot or sample each time. The samples were measured on NC filters at both room temperature and 77K. Global analysis (17) of the data was performed using the TIMP-based Glotaran program (58), in order to identify the spectral components in the fluorescence signal (see SI methods).

Solution Small angle X-ray and Neutron scattering

High-resolution small-angle X-ray scattering (SAXS) was performed as described in (59). Small-angle neutron scattering (SANS) was performed at the KWS-2 instrument operated by JCNS at the Heinz Maier-Leibnitz Zentrum (MLZ), Garching, Germany ((60, 61) and SI methods). The scattering intensity, *I*, as a function of the magnitude of the momentum transfer vector, *q*, was then plotted and analyzed to determine the typical repeat distances (RDs) between membranes (62).

Acknowledgments

This work was supported by the ISF-UGC grant (2733/16) awarded to NK and the MOST-NSC grant awarded to NK and YP. RRC was supported by BioSolar Cells, co-financed by the Dutch Ministry of Economic Affairs and the FOM, part of The Netherlands Organization for Scientific Research (project 10TBSC24-3). GG and MD were supported by the National Research

Development and Innovation Office of Hungary (OTKA K 112688 and GINOP-2.3.2-15-2016-00058 and PD 121243).

1. Belnap J (2013) Microbiology. Some like it hot, some not. *Science* 340(6140):1533–4.
2. Garcia-Pichel F, Johnson SL, Youngkin D, Belnap J (2003) Small-Scale Vertical Distribution of Bacterial Biomass and Diversity in Biological Soil Crusts from Arid Lands in the Colorado Plateau. *Microb Ecol* 46(3):312–321.
3. Raanan H, et al. (2016) Simulated soil crust conditions in a chamber system provide new insights on cyanobacterial acclimation to desiccation. *Environ Microbiol* 18(2):414–426.
4. Ohad I, Raanan H, Keren N, Tchernov D, Kaplan A (2010) Light-induced changes within photosystem II protects Microcoleus sp. in biological desert sand crusts against excess light. *PLoS One* 5(6):e11000.
5. Ohad I, et al. (2005) Inactivation of photosynthetic electron flow during desiccation of desert biological sand crusts and Microcoleus sp.-enriched isolates. *Photochem Photobiol Sci* 4:977–982.
6. Harel Y, Ohad I, Kaplan A (2004) Activation of photosynthesis and resistance to photoinhibition in cyanobacteria within biological desert crust. *Plant Physiol* 136(2):3070–3079.
7. Bar-Eyal L, et al. (2015) An easily reversible structural change underlies mechanisms enabling desert crust cyanobacteria to survive desiccation. *Biochim Biophys Acta - Bioenerg* 1847(10):1267–1273.
8. Rajeev L, et al. (2013) Dynamic cyanobacterial response to hydration and dehydration in a desert biological soil crust. *ISME J* 7(11):2178–2191.
9. Charuvi D, et al. (2015) Photoprotection conferred by changes in photosynthetic protein levels and organization during dehydration of a homoiochlorophyllous resurrection plant. *Plant Physiol* 167(4):1554–1565.
10. Kranner I, Birtic S (2005) A modulating role for antioxidants in desiccation tolerance. *Integr Comp Biol* 45:734–740.
11. Dinakar C, Bartels D (2013) Desiccation tolerance in resurrection plants: new insights from transcriptome, proteome and metabolome analysis. *Front Plant Sci* 4:482.
12. Barak S, Farrant JM (2016) Extremophyte adaptations to salt and water deficit stress. *Funct Plant Biol* 43(7):v–x.
13. Campbell D a, Hurry V, Clarke AK, Gustafsson P, Oquist G (1998) Chlorophyll fluorescence analysis of cyanobacterial photosynthesis and acclimation. *Microbiol Mol Biol Rev* 62(3):667–683.
14. Maxwell K, Johnson GN (2000) Chlorophyll fluorescence--a practical guide. *J Exp Bot* 51(345):659–668.
15. Adir N (2005) Elucidation of the molecular structures of components of the phycobilisome: Reconstructing a giant. *Photosynth Res* 85(1):15–32.
16. Tian L, et al. (2011) Site, rate, and mechanism of photoprotective quenching in cyanobacteria. *J Am Chem Soc* 133(45):18304–18311.
17. Van Stokkum IHM, Larsen DS, Van Grondelle R (2004) Global and target analysis of time-resolved spectra. *Biochim Biophys Acta - Bioenerg* 1657(2–3):82–104.
18. Debreczeny MP, Sauer K, Jianhui Z, Bryant DA (1993) Monomeric C-Phycocyanin at Room Temperature and 77 K: Resolution of the Absorption and Fluorescence Spectra of the Individual Chromophores and the Energy-Transfer Rate Constants. *J Phys Chem* 97:9852–9862.
19. Kupka M, Scheer H (2008) Unfolding of C-phycocyanin followed by loss of non-covalent chromophore-protein interactions. 1. Equilibrium experiments. *Biochim Biophys Acta - Bioenerg* 1777(1):94–103.
20. Tian L, et al. (2012) Picosecond kinetics of light harvesting and photoprotective quenching in wild-type and mutant phycobilisomes isolated from the cyanobacterium Synechocystis PCC 6803. *Biophys J* 102(7):1692–1700.
21. Kirilovsky D (2015) Modulating energy arriving at photochemical reaction centers: Orange carotenoid protein-related photoprotection and state transitions. *Photosynth Res* 126(1):3–17.
22. Kirilovsky D, et al. (2016) Cyanobacterial photoprotection by the orange carotenoid protein. *Nat Plants* 2(12):16180.
23. Boulay C, Wilson A, D'Haene S, Kirilovsky D (2010) Identification of a protein required for recovery of full antenna capacity in OCP-related photoprotective mechanism in cyanobacteria. *Proc Natl Acad Sci USA* 107(25):11620–11625.
24. Wilson A, et al. (2006) A soluble carotenoid protein involved in phycobilisome-related energy dissipation in cyanobacteria. *Plant Cell* 18:992–1007.
25. Harris D, et al. (2016) Orange carotenoid protein burrows into the phycobilisome to provide photoprotection. *Proc Natl Acad Sci USA* 113(12):E1655-62.
26. Rolczynski BS, Navotnaya P, Sussman HR, Engel GS (2016) Cysteine-mediated mechanism disrupts energy transfer to prevent photooxidation. *Proc Natl Acad Sci USA* 113(31):8562–8564.
27. Chen H-YS, Liberton M, Pakrasi HB, Niedzwiedzki DM (2017) Reevaluating the Mechanism of Excitation Energy Regulation in Iron-Starved Cyanobacteria. *Biochim Biophys Acta-Bioenerg*.
28. Chen M, Floetenmeyer M, Bibby TS (2009) Supramolecular organization of phycobiliproteins in the chlorophyll d-containing cyanobacterium Acaryochloris marina. *FEBS Lett* 583(15):2535–9.
29. Ünnep R, et al. (2014) The ultrastructure and flexibility of thylakoid membranes in leaves and isolated chloroplasts as revealed by small-angle neutron scattering. *Biochim Biophys Acta-Bioenerg* 1837(9):1572–1580.
30. Nagy G, et al. (2011) Reversible membrane reorganizations during photosynthesis in vivo: revealed by small-angle neutron scattering. *Biochem J* 436:225–230.
31. Liberton M, et al. (2013) Organization and flexibility of cyanobacterial thylakoid membranes examined by neutron scattering. *J Biol Chem* 288(5):3632–40.
32. Unnep R, Nagy G, Markó M, Garab G (2014) Monitoring thylakoid ultrastructural changes in vivo using small-angle neutron scattering. *Plant Physiol Biochem* 81:1–11.
33. Kirchhoff H, et al. (2011) Dynamic control of protein diffusion within the granal thylakoid lumen. *Proc Natl Acad Sci* 108(50):20248–20253.
34. Eisenberg I, et al. (2017) Regulating the Energy Flow in a Cyanobacterial Light Harvesting Antenna Complex. *J Phys Chem B*.
35. Kobayashi T (2012) J-Aggregates (World Scientific Publisihng, Singapure).
36. Clark J, Silva C, Friend RH, Spano FC (2007) Role of intermolecular coupling in the photophysics of disordered organic semiconductors: Aggregate emission in regioregular polythiophene. *Phys Rev Lett* 98(20):1–4.
37. Chin a. W, et al. (2013) The role of non-equilibrium vibrational structures in electronic coherence and recoherence in pigment–protein complexes. *Nat Phys* 9(2):113–118.
38. Rebentrost P, Mohseni M, Kassal I, Lloyd S, Aspuru-Guzik A (2009) Environment-assisted quantum transport. *New J Phys* 11. doi:10.1088/1367-2630/11/3/033003.
39. Scholes GD (2010) Quantum-coherent electronic energy transfer: Did nature think of it first? *J Phys Chem Lett* 1(1):2–8.
40. Ishizaki A, Fleming GR (2009) Theoretical examination of quantum coherence in a photosynthetic system at physiological temperature. *Proc Natl Acad Sci USA* 106(41):17255–17260.
41. van Amerongen H, van Grondelle R (2001) Understanding the Energy Transfer Function of LHCII, the Major Light-Harvesting Complex of Green Plants. *J Phys Chem B* 105(3):604–617.
42. Gradinaru CC, et al. (1998) The flow of excitation energy in LHCII monomers: implications for the structural model of the major plant antenna. *Biophys J* 75(6):3064–77.
43. Moix JM, Khasin M, Cao J (2013) Coherent quantum transport in disordered systems: I. the influence of dephasing on the transport properties and absorption spectra on one-dimensional systems. *New J Phys* 15. doi:10.1088/1367-2630/15/8/085010.
44. Zhong X, Zhao Y, Cao J (2014) Coherent quantum transport in disordered systems: II. Temperature dependence of carrier diffusion coefficients from the time-dependent wavepacket diffusion method. *New J Phys* 16. doi:10.1088/1367-2630/16/4/045009.
45. Tamary E, et al. (2012) Structural and functional alterations of cyanobacterial phycobilisomes induced by high-light stress. *Biochim Biophys Acta* 1817:319–327.
46. Johnson MP, et al. (2011) Photoprotective energy dissipation involves the reorganization of photosystem II light-harvesting complexes in the grana membranes of spinach chloroplasts. *Plant Cell* 23:1468–1479.
47. Horton P, Wentworth M, Ruban A (2005) Control of the light harvesting function of chloroplast membranes: The LHCII-aggregation model for non-photochemical quenching. *FEBS Lett* 579(20):4201–4206.
48. Bassi R, Silvestri M, Dainese P, Moya I, Giacometti GM (1991) Effects of a non-ionic detergent on the spectral properties and aggregation state of the light-harvesting chlorophyll a/b protein complex (LHCII). *J Photochem Photobiol B Biol* 9(3–4):335–353.
49. Barzda V, Garab G, Gulbinas V, Valkunas L (1996) Evidence for long-range excitation energy migration in macroaggregates of the chlorophyll a/b light-harvesting antenna complexes. *Biochim Biophys Acta-Bioenerg* 1273(3):231–236.
50. Chmeliov J, et al. (2016) The nature of self-regulation in photosynthetic light-harvesting antenna. *Nat Plants* 2:16045.
51. Kirchhoff H, Hinz HJ, Rösgen J (2003) Aggregation and fluorescence quenching of chlorophyll a of the light-harvesting complex II from spinach in vitro. *Biochim Biophys Acta-Bioenerg* 1606(1–3):105–116.
52. Dinc E, et al. (2016) LHCSR1 induces a fast and reversible pH-dependent fluorescence quenching in LHCII in *Chlamydomonas reinhardtii* cells. *Proc Natl Acad Sci USA* 7673-7678.
53. Ruban A V., et al. (2007) Identification of a mechanism of photoprotective energy dissipation in higher plants. *Nature* 450(7169):575–578.
54. Vicré M, Farrant JM, Driouich A (2004) Insights into the cellular mechanisms of desiccation tolerance among angiosperm resurrection plant species. *Plant, Cell Environ* 27(11):1329–1340.
55. Clarke J, Wilhelm FK (2008) Superconducting quantum bits. *Nature* 453:1031–1042.
56. van Stokkum IHM, van Oort B, van Mourik F, Gobets B, van Amerongen H (2008) (Sub)-picosecond spectral evolution of fluorescence studied with a synchroscan streak-camera system and target analysis. *Biophysical Techniques in Photosynthesis*, eds Aartsma TJ, Matysik J (Springer Netherlands), pp 223–240.
57. Chukhutsina V, Bersanini L, Aro E-M, van Amerongen H (2015) Cyanobacterial Light-Harvesting Phycobilisomes Uncouple From Photosystem I During Dark-To-Light Transitions. *Sci Rep* 5:14193.
58. Snellenburg JJ, Laptenok SP, Seger R, Mullen KM, van Stokkum IHM (2012) Glotaran : A Java -Based Graphical User Interface for the R Package TIMP. *J Stat Softw* 49(3).
59. Nadler M, et al. (2011) Following the structural changes during zinc-induced crystallization of charged membranes using time-resolved solution X-ray scattering. *Soft Matter* 7(4):1512.
60. Nagy G, et al. (2014) Chloroplast remodeling during state transitions in Chlamydomonas reinhardtii as revealed by noninvasive techniques in vivo. *Proc Natl Acad Sci USA* 111(13):5042–7.
61. Radulescu A, et al. (2016) Studying Soft-matter and Biological Systems over a Wide Length-scale from Nanometer and Micrometer Sizes at the Small-angle Neutron Diffractometer KWS-2. *J Vis Exp* (118):1–23.
62. Steiner A, et al. (2012) Entropic attraction condenses like-charged interfaces composed of self-assembled molecules. *Langmuir* 28:2604–2613.
63. Gussakovsky, E. E., Barzda, V., Shahak, Y., & Garab, G. (1997). Irreversible disassembly of chiral macrodomains in thylakoids due to photoinhibition. *Photosynth Res*, 51(2), 119-126.